

A hybrid sliding mode control and bounded variable least squares framework for an eight-cable-driven parallel robot

Huu Phuoc Nguyen¹, Toan Phat Dinh¹, Duc Manh Nguyen¹, Duc Huy Nguyen¹, Duc Chi Nguyen¹ and Thi Van Anh Nguyen^{1,*}

¹*School of Electrical and Electronic Engineering, Hanoi University of Science and Technology*

**Corresponding author E-mail: anh.nguyenthivan1@hust.edu.vn*

DOI: <https://doi.org/10.64032/mca.v30i3.439>

Abstract

Cable-driven parallel robots (CDPRs) have attracted considerable attention due to their advantages in large workspace, lightweight structure, and high dynamic performance. However, the control of eight-cable-driven parallel robot systems remains challenging because of their nonlinear and strongly coupled dynamics, as well as the requirement that cable tensions must remain within feasible bounds during operation. This paper proposes a hybrid control framework combining Sliding Mode Control (SMC) and Bounded Variable Least Squares (BVLS) for trajectory tracking and cable tension distribution of an eight-cable-driven parallel robot, where the SMC strategy is employed to achieve robust tracking performance under nonlinear and uncertain operating conditions. The desired control wrench generated by the SMC is subsequently allocated into feasible cable tensions through the BVLS algorithm, which determines an optimal least-squares tension solution subject to bounded cable tension constraints. Simulation results demonstrate that the proposed control framework achieves fast transient response and high tracking accuracy for both translational and rotational motions, while all cable tensions remain within the prescribed feasible bounds.

Keywords: *Cable-driven parallel robot; Sliding mode control; Bounded variable least squares; Trajectory tracking control; Tension allocation*

1. Introduction

Cable-driven parallel robots (CDPRs) have attracted significant attention in recent years due to their advantages in large workspace, lightweight mechanical structure, high payload-to-weight ratio, and high-speed motion capability. Compared with conventional rigid-link parallel robots, CDPRs utilize cables instead of rigid actuators to manipulate the end-effector, thereby reducing the moving inertia and improving operational flexibility [1], [2]. Owing to these characteristics, CDPR systems have been widely investigated in various applications such as industrial automation, large-scale manufacturing, rehabilitation systems [3], camera positioning platforms [4], and cooperative robotic manipulation [5]. Numerous studies have been devoted to the modeling, control, and trajectory tracking of CDPR systems [6], [7]. For example, Nguyen et al. [8] proposed a PSO-tuned sliding mode control strategy for trajectory tracking and orientation stabilization of a planar CDPR. In that work, the robot motion was restricted to a two-dimensional workspace, where the end-effector position and orientation were described by a limited set of planar coordinates. Although promising tracking performance was achieved, the considered system involved a lower-dimensional dynamic model and a relatively simpler cable tension distribution problem compared with spatial CDPR configurations. In contrast, this study considers an eight-cable-driven parallel robot capable of full six-degree-of-freedom motion in a three-dimensional workspace. While this configuration provides greater operational flexibility and manipulation capability than planar CDPRs, it also introduces substantially more complex dynamics. The translational and rotational motions of the end-effector are strongly

coupled, and the redundant actuation structure gives rise to nonunique cable tension solutions. In addition, because cables can only exert tensile forces, all cable tensions must remain within admissible positive bounds throughout the motion process. These characteristics make robust trajectory tracking and feasible tension allocation challenging problems in practical CDPR applications [9].

To address these challenges, numerous control approaches have been proposed for CDPR systems. Conventional feedback controllers, including PID [10], [11] and LQR [12], have been widely utilized due to their straightforward implementation and low computational burden. However, their performance may degrade significantly in the presence of nonlinear dynamics, parameter uncertainties, and external disturbances. In recent years, advanced intelligent and nonlinear control strategies have attracted increasing attention for cable-driven robotic systems. Among these methods, fuzzy logic controllers [13], [14] have demonstrated effectiveness in handling uncertain nonlinear dynamics without requiring highly accurate mathematical models. Neural network-based approaches [15], [16] further improve adaptive approximation capability through online learning mechanisms. In addition, hybrid intelligent methods such as fuzzy neural networks and neuro-fuzzy systems [17], [18] combine the reasoning capability of fuzzy systems with the learning ability of neural networks to enhance control adaptability and tracking performance. Nevertheless, these intelligent control approaches often require complicated parameter tuning procedures, large computational resources, and stability analysis, which may limit their applicability in real-time control of high-speed CDPR systems. Furthermore, optimization-based and learning-based approaches, including

reinforcement learning [19] and evolutionary algorithms [20], have also been investigated for trajectory tracking and cable tension optimization. Although these methods show promising performance for complex nonlinear systems, they generally involve extensive training procedures and high computational complexity, making real-time implementation challenging for practical robotic applications.

Compared with advanced intelligent control approaches, Sliding Mode Control (SMC) [21], [22] provides a relatively simple yet robust control structure with favorable disturbance rejection capability and fast convergence properties, making it suitable for real-time trajectory tracking of 6-DOF CDPRs [23], [24]. The main principle of SMC is to drive the system trajectories toward a predefined sliding surface and maintain the system motion on this manifold to ensure stable tracking performance [25]. Owing to its robustness against model uncertainties and external disturbances, SMC has demonstrated effectiveness for nonlinear and strongly coupled robotic systems. Therefore, SMC is adopted in this study to achieve stable and accurate trajectory tracking performance for the proposed CDPR system.

Although the proposed SMC scheme can provide a desired control wrench for robust trajectory tracking, this wrench must be converted into feasible cable tensions before being applied to the CDPR. Such a conversion is nontrivial because the system is redundantly actuated, meaning that multiple cable tension distributions can generate the same wrench. In addition, cable tensions must satisfy positivity and boundedness constraints throughout the motion process. Consequently, an effective tension allocation strategy is essential to bridge the gap between the control wrench generated by SMC and the actual cable actuation commands applied to the robot. Various cable tension allocation methods have been investigated for redundantly actuated CDPRs. Traditional pseudo-inverse [26] and null-space [27], [28] approaches are widely used due to their simplicity and fast computation. However, they do not explicitly enforce cable tension bounds, and additional procedures are often required to prevent cable slackness or excessive tensions. Consequently, feasible solutions cannot always be guaranteed, particularly when the robot operates near workspace boundaries or under large external disturbances. More recently, optimization-based techniques such as quadratic programming (QP) [29] have been introduced to explicitly handle cable tension constraints. By incorporating linear inequality constraints into the optimization process, QP can generate feasible tension solutions while satisfying additional objectives. However, solving a constrained quadratic optimization problem at every control step may increase computational requirements, especially in real-time applications involving high control frequencies. To overcome these limitations, the Bounded Variable Least Squares (BVLS)[30] method is employed in this work. BVLS directly computes cable tensions while explicitly satisfying prescribed lower and upper tension bounds. Compared with pseudo-inverse-based methods, BVLS guarantees constraint-compliant solutions, and compared with general QP formulations, it offers a simpler least-squares framework with lower computational burden. These characteristics make BVLS particularly suitable for real-time cable tension allocation in redundantly actuated CDPRs.

Although considerable progress has been made in the control of CDPR systems, most existing studies focus either on tra-

jectory tracking performance or on cable tension allocation as separate problems. Furthermore, many SMC-based approaches have been developed for planar or lower-dimensional CDPR configurations, while limited attention has been devoted to integrating robust trajectory tracking and constraint-aware tension allocation for redundantly actuated spatial 6-DOF CDPRs. Consequently, achieving accurate tracking performance while simultaneously guaranteeing feasible bounded cable tensions remains a challenging issue. These challenges motivate the present study. Based on the above considerations, this study proposes a hybrid control framework combining SMC and BVLS for a 6-DOF eight-cable-driven parallel robot. First, a complete dynamic model describing both translational and rotational motions of the end-effector is established. Subsequently, the SMC strategy is designed to achieve robust and accurate trajectory tracking under nonlinear and coupled system dynamics. The desired control wrench generated by the SMC is then transformed into feasible cable tensions through the BVLS algorithm while satisfying bounded tension constraints. Finally, simulation results verify the effectiveness of the proposed framework in terms of tracking performance and cable tension feasibility.

2. Modeling

The considered eight-cable-driven parallel robot (8-CDPR) consists of a rigid end effector actuated by eight cables attached between the fixed base frame and the moving platform, as illustrated in Fig. 1. The dimensions of the fixed base frame are denoted by $m \times n \times k$, while the dimensions of the end effector are represented by $p \times q \times r$. A global coordinate system $Oxyz$ is established at the base attachment point C_4 , ensuring that the workspace of the end effector lies entirely in the nonnegative coordinate region.

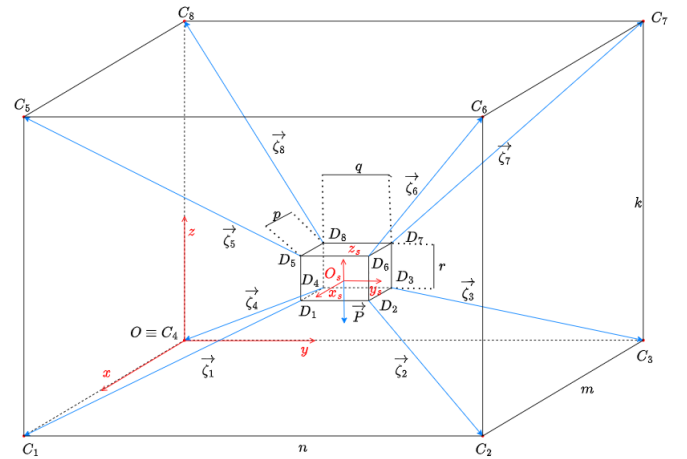


Figure 1: Eight-cable driven parallel robot model

To simplify the dynamic modeling and controller design, the following assumptions are considered.

Assumption 1. *The eight cables are assumed to remain perfectly straight during operation, while cable sagging effects are neglected due to the relatively short cable spans.*

Assumption 2. *Each cable can only transmit tensile force. Therefore, the cable tension ζ_i is always nonnegative and acts along the direction from the base attachment point C_i to the corresponding platform attachment point D_i .*

The end effector is modeled as a rigid body with six degrees of freedom, consisting of three translational motions and three rotational motions. A local coordinate frame, denoted by $O_s x_s y_s z_s$, is attached to the center point O_s of the end effector, while the global reference frame is defined as $Oxyz$. The translational motion of the end effector is described by the position vector of O_s in the global frame, expressed as $(x_{O_s}, y_{O_s}, z_{O_s})$.

The rotational motion is represented by three orientation angles (ϕ_x, ϕ_y, ϕ_z) corresponding to roll, pitch, and yaw motions, respectively. Specifically, ϕ_x denotes the rotational deviation around the x -axis, ϕ_y represents the rotational deviation around the y -axis, and ϕ_z describes the rotational deviation around the z -axis between the local frame $O_s x_s y_s z_s$ and the global frame $Oxyz$.

Accordingly, the generalized coordinate vector of the end effector is defined as

$$\mathbf{X} = [x_{O_s} \ y_{O_s} \ z_{O_s} \ \phi_x \ \phi_y \ \phi_z]^T. \quad (1)$$

Using the Newton–Euler formulation, the dynamic model of the 8-CDPR can be expressed as follows:

$$\begin{cases} m\ddot{\lambda} = \sum_{i=1}^8 \vec{\zeta}_i + \vec{P} + \vec{F}_d \\ T\ddot{\phi} + \dot{\phi} \times (T\dot{\phi}) = \sum_{i=1}^8 \vec{\rho}_i \times \vec{\zeta}_i + \vec{\zeta}_d \end{cases} \quad (2)$$

Here, T and m denote the inertia matrix and mass of the end effector, respectively. The force exerted by the i -th cable is represented by $\vec{\zeta}_i$, whose associated moment arm is defined by $\vec{\rho}_i$. The gravity vector is expressed as \vec{P} , while \vec{F}_d and $\vec{\zeta}_d$ correspond to the external force and moment disturbances acting on the system. Moreover, $\ddot{\lambda}$ and $\ddot{\phi}$ indicate the linear and angular accelerations of the end effector.

In the fixed frame $Oxyz$, the base attachment points are represented by the vectors $\vec{\lambda}_{C_i}$ and $\vec{\lambda}_{D_i}$. The spatial position of the end-effector's center point O_s is defined by the translation vector $\vec{\lambda} = [x_{O_s} \ y_{O_s} \ z_{O_s}]^T$. For the eight actuating cables ($i = 1, 2, \dots, 8$), their attachment nodes on the platform are assigned local coordinates $\lambda_{D_{i,s}} = [x_{D_{i,s}} \ y_{D_{i,s}} \ z_{D_{i,s}}]^T$ relative to the moving frame. To determine their corresponding coordinates $\lambda_{D_i} = [x_{D_i} \ y_{D_i} \ z_{D_i}]^T$ within the global frame $Oxyz$, a coordinate transformation is applied. By integrating the translation vector λ and the rotation matrix \mathcal{R} , the positions of the attachment points are calculated as follows:

$$\lambda_{D_i} = \mathcal{R}\lambda_{D_{i,s}} + \lambda \quad (3)$$

where \mathcal{R} denotes the 3×3 rotation matrix that defines the orientation mapping from the moving end-effector frame back to the global base frame, which is given by:

$$\mathcal{R} = \begin{bmatrix} c\phi_z c\phi_y & c\phi_z s\phi_y s\phi_x - s\phi_z c\phi_x & c\phi_z s\phi_y c\phi_x + s\phi_z s\phi_x \\ s\phi_z c\phi_y & s\phi_z s\phi_y s\phi_x + c\phi_z c\phi_x & s\phi_z s\phi_y c\phi_x - c\phi_z s\phi_x \\ -s\phi_y & c\phi_y s\phi_x & c\phi_y c\phi_x \end{bmatrix} \quad (4)$$

and $c\phi_x = \cos(\phi_x)$, $c\phi_y = \cos(\phi_y)$, $c\phi_z = \cos(\phi_z)$, $s\phi_x = \sin(\phi_x)$, $s\phi_y = \sin(\phi_y)$, $s\phi_z = \sin(\phi_z)$.

The directional unit vectors for each cable are obtained via normalization and calculated using the following equation:

$$\vec{u}_i = \frac{\vec{D}_i \vec{C}_i}{|\vec{D}_i \vec{C}_i|} = \frac{\vec{C}_i - \vec{D}_i}{|\vec{C}_i - \vec{D}_i|} \quad (5)$$

the moment arm vector $\vec{\rho}_i$ is determined through the cross product defined below:

$$\vec{\rho}_i = \mathcal{R}\lambda_{D_{i,s}} \times \vec{u}_i \quad (6)$$

By consolidating the six degrees of freedom defined in (1), the system of equations from (2) to be compactly expressed in matrix form:

$$\mathbf{A}\ddot{\mathbf{X}} + \mathbf{Q}\dot{\mathbf{X}} = \mathbf{U} + \mathbf{P} \quad (7)$$

where $\mathbf{U} = \mathbf{B}\zeta \in \mathbb{R}^{6 \times 1}$ denotes the generalized control input vector consisting of the resultant translational forces and rotational moments acting on the end effector.

$$\mathbf{A} = \begin{bmatrix} m & 0 \\ 0 & T \end{bmatrix}, \quad \mathbf{P} = \begin{bmatrix} \vec{P} \\ 0 \end{bmatrix}, \quad \mathbf{Q} = \begin{bmatrix} 0 & 0 \\ 0 & -(T\dot{\phi})^\times \end{bmatrix}, \quad \mathbf{H} = \begin{bmatrix} \vec{\zeta}_d \\ \vec{F}_d \end{bmatrix}$$

$$\mathbf{B} = \begin{bmatrix} u_1 & u_2 & \cdots & u_7 & u_8 \\ \vec{\rho}_1 & \vec{\rho}_2 & \cdots & \vec{\rho}_7 & \vec{\rho}_8 \end{bmatrix}, \quad \zeta = [\zeta_1 \ \zeta_2 \ \cdots \ \zeta_7 \ \zeta_8]^T,$$

$$T = \begin{bmatrix} T_{xx} & 0 & 0 \\ 0 & T_{yy} & 0 \\ 0 & 0 & T_{zz} \end{bmatrix}.$$

where $T_{xx} = \frac{m}{12}(q^2 + r^2)$, $T_{yy} = \frac{m}{12}(p^2 + r^2)$, and $T_{zz} = \frac{m}{12}(p^2 + q^2)$. To construct the Coriolis force matrix N , the mathematical operator $()^\times$ is applied [31], the matrix is formulated as follows:

$$(T\dot{\phi})^\times = \begin{bmatrix} 0 & -T_{zz}\dot{\phi}_z & T_{yy}\dot{\phi}_y \\ T_{zz}\dot{\phi}_z & 0 & -T_{xx}\dot{\phi}_x \\ -T_{yy}\dot{\phi}_y & T_{xx}\dot{\phi}_x & 0 \end{bmatrix} \quad (8)$$

3. Controller design

This section presents a hybrid control strategy for the 6-DOF cable-driven parallel robot, in which Sliding Mode Control (SMC) is employed to ensure robust trajectory tracking, while the Bounded Variable Least Squares (BVLS) method is utilized for cable tension distribution under tension constraints.

3.1 Sliding Mode Control

To evaluate the tracking performance, the tracking error vector e is defined as the deviation between the actual state and the desired state:

$$e = \mathbf{X} - \mathbf{X}_d \quad (9)$$

where \mathbf{X}_d denotes the desired state vector.

To guarantee the asymptotic convergence of the tracking error e to zero, a sliding surface s is defined as follows:

$$s = \mathbf{C}e + \dot{e} \quad (10)$$

where \mathbf{C} is a positive diagonal matrix.

The sliding mode control law \mathbf{U} is designed as follows:

$$\mathbf{U} = \mathbf{A} (\ddot{\mathbf{X}}_d - \alpha \text{sign}(s) - \mathbf{C}\dot{e}) - \mathbf{P} + \mathbf{Q}\dot{\mathbf{X}} \quad (11)$$

where α is a positive switching gain diagonal matrix.

Taking the first time derivative of the sliding surface yields:

$$\dot{s} = \mathbf{C}\dot{e} + \ddot{e} \quad (12)$$

The Lyapunov function candidate is chosen as follows:

$$V = \frac{1}{2}s^2 \quad (13)$$

Taking the first time derivative of the Lyapunov function yields:

$$\dot{V} = s^T \dot{s} = s^T (\mathbf{C}\dot{e} + \ddot{e}) = s^T (\mathbf{C}\dot{e} + \ddot{\mathbf{X}} - \ddot{\mathbf{X}}_d)$$

By substituting the system dynamics (2) into the equation above, the derivative of the Lyapunov function becomes:

$$\dot{V} = s^T [\mathbf{C}\dot{e} + \mathbf{A}^{-1} (\mathbf{U} + \mathbf{P} - \mathbf{Q}\dot{\mathbf{X}}) - \ddot{\mathbf{X}}_d] \quad (14)$$

Substituting the proposed control law (11) into (14) yields:

$$\dot{V} = s^T (-\alpha \text{sign}(s)) = -\alpha \|s\|_1 \leq 0$$

Since $V > 0$ for $s \neq 0$ and $\dot{V} \leq 0$, the closed-loop system is asymptotically stable according to Lyapunov's stability theorem. This mathematically guarantees that the system states will converge to the sliding surface $s = 0$ in finite time, subsequently ensuring that the tracking error e asymptotically converges to zero.

Remark 1. A well-known drawback of the conventional SMC is the chattering effect caused by the discontinuous sign switching logic. To alleviate this high-frequency oscillation, the discontinuous sign operator is substituted with a continuous saturation function, $\text{sat}(x)$. This function is mathematically defined as follows:

$$\text{sat}(x) = \begin{cases} 1, & x > \Delta \\ \frac{1}{\Delta}x, & -\Delta \leq x \leq \Delta \\ -1, & x < -\Delta \end{cases} \quad (15)$$

where Δ is a small positive design constant.

3.2 Bounded Variable Least Squares

The cable tension distribution problem is solved using the Bounded Variable Least Squares (BVLS) method, which determines the cable tensions while satisfying the physical constraints of the cable driven system.

In general, the BVLS formulation can be expressed as:

$$\mathbf{A}x = \mathbf{B} \quad (16)$$

subject to the variable bounds

$$x_{\min} \leq x \leq x_{\max} \quad (17)$$

where $\mathbf{A} \in \mathbb{R}^{p \times q}$ is the coefficient matrix, $x \in \mathbb{R}^{q \times 1}$ denotes the unknown variable vector, and $\mathbf{B} \in \mathbb{R}^{p \times 1}$ represents the desired output vector.

By combining the force and moment equilibrium equations, the cable tensions can be formulated as:

$$\begin{cases} u_1 \zeta_1 + u_2 \zeta_2 + \dots + u_8 \zeta_8 = \mathcal{F}_{\text{total}} \\ \rho_1 \zeta_1 + \rho_2 \zeta_2 + \dots + \rho_8 \zeta_8 = \mathcal{M} \end{cases} \quad (18)$$

which can be rewritten in compact form as

$$\mathcal{W}\zeta = \mathcal{U} \quad (19)$$

where $\mathcal{W} = \mathbf{B} \in \mathbb{R}^{6 \times 8}$ is the wrench matrix and $\mathcal{U} = \begin{bmatrix} \mathcal{F}_{\text{total}} \\ \mathcal{M} \end{bmatrix} \in \mathbb{R}^{6 \times 1}$ is the desired control wrench vector.

Since cables can only generate tensile forces, the cable tensions are constrained by

$$0 \leq \zeta_i \leq \zeta_{i,\max}, \quad i = 1, 2, \dots, 8 \quad (20)$$

Accordingly, the cable tension vector is obtained by solving the constrained least squares problem

$$\min_{\zeta} \|\mathcal{W}\zeta - \mathcal{U}\|_2^2 \quad (21)$$

subject to the bounds in (20).

By solving the constrained system defined in (20) and (21) via the BVLS algorithm [32], the optimal control tension ζ_i for each cable is computed, thereby guaranteeing accurate trajectory tracking.

4. Simulation results

This section presents the simulation results of the proposed SMC-BVLS control framework for the 8-CDPR. The simulations are carried out under nominal operating conditions with a supporting frame spanning $2\text{m} \times 2\text{m} \times 4\text{m}$ along the x -, y -, and z -axes, respectively. The end-effector is modeled as a lightweight rigid body with dimensions of $0.2\text{m} \times 0.2\text{m} \times 0.2\text{m}$ and a mass of 10kg . The gravitational acceleration adopted in the simulation is 9.8m/s^2 . The initial position of the end-effector is specified as $[1 \ 1 \ 0.5]^T$, while the initial orientation angles about the O_x , O_y , and O_z axes are all set to zero. The reference trajectory consists of an initial vertical ascent followed by a circular motion with a radius of $R = 0.5\text{m}$ at a constant height, before converging to a final equilibrium point. Moreover, the cable tensions are constrained within the range $0 \leq T_i \leq 200\text{N}$.

Based on this simulation setup, the performance of the proposed control framework for the 8-CDPR is evaluated. To demonstrate its effectiveness, its tracking performance is validated through a comparison with the conventional SMC-based Null Space Method under two cases:

- Case 1: Trajectory tracking performance under ideal nominal conditions, isolated from external disturbances and model uncertainties.
- Case 2: Trajectory tracking performance subjected to continuous external disturbances to evaluate the robustness of the control schemes.

To ensure a fair and objective comparison, the SMC parameters used in both the proposed controller and the SMC-based Null Space Method (SMC-NSM) were selected identically throughout all simulations. Specifically, the sliding surface matrix and switching gain matrix were chosen as $\mathbf{C} =$

$diag([4, 4, 4, 3, 3, 3])$ and $\alpha = diag([8, 8, 8, 5, 5, 5])$. These parameters were maintained unchanged for both control schemes under all simulation scenarios, including ideal and noisy operating conditions. Therefore, the performance differences observed in the simulations can be directly associated with the effectiveness of the control strategies themselves, since both methods were evaluated under identical parameter settings.

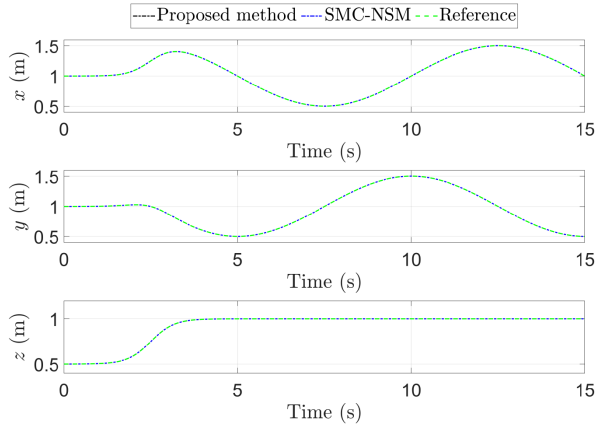


Figure 2: Case 1: Translational motions of the cable-driven parallel robot under nominal condition.

From Figure 2, it can be clearly observed that both controllers are capable of tracking the prescribed Cartesian trajectory in the x-, y-, and z-directions. Nevertheless, the proposed controller demonstrates substantially improved tracking precision throughout the entire motion process. The tracking curves generated by the proposed method almost completely overlap the reference trajectories, indicating excellent dynamic consistency and highly accurate position regulation.

A more detailed observation of the enlarged regions reveals that the proposed controller produces significantly smaller local tracking deviations during transient motion. This characteristic is particularly important because transient phases correspond to regions where the robot experiences strong non-linear coupling, rapid acceleration changes, and dynamic interaction among cables. In such situations, conventional sliding-mode-based methods generally suffer from residual oscillations due to discontinuous control actions. The proposed controller, however, maintains smooth convergence and suppresses oscillatory behavior effectively.

The quantitative results shown in Table 1 further confirm these observations. Under ideal conditions, the proposed controller achieves RMSE values of $2.8566 \cdot 10^{-4}$ m, $2.2338 \cdot 10^{-4}$ m, and $1.7951 \cdot 10^{-4}$ m for the x-, y-, and z-axes, respectively. Compared with the SMC-NSM method, these values are consistently lower, indicating improved steady-state precision. The most remarkable improvement appears in the z-direction, where the tracking error is reduced by several orders of magnitude. This result indicates that the proposed control framework possesses superior vertical stabilization capability, which is essential in cable-driven robots because vertical motion is strongly influenced by gravity, cable tension redistribution, and coupled platform dynamics.

The maximum error results provide additional insight into transient performance. The proposed method limits the maximum Cartesian deviations to less than 10^{-3} m in all translational coordinates, whereas the SMC-NSM controller pro-

duces larger peak deviations, especially in the x-direction. This demonstrates that the proposed strategy not only improves average tracking precision but also enhances transient stability during aggressive trajectory changes.

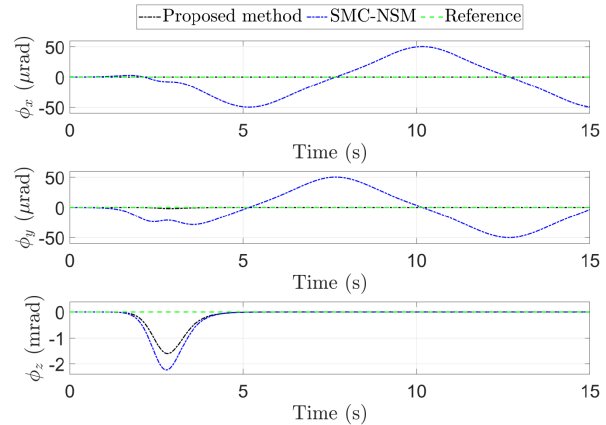


Figure 3: Case 1: Rotational motions of the cable-driven parallel robot under nominal condition.

The rotational tracking responses shown in Figure 3 further highlight the superiority of the proposed approach. The rotational coordinates ϕ_x , ϕ_y and ϕ_z converge rapidly toward the equilibrium point with nearly negligible oscillation amplitudes. In contrast, the SMC-NSM controller exhibits visible oscillatory behavior during both transient and steady-state phases.

The difference between the two methods becomes more evident in the ϕ_z response. While the proposed controller maintains a smooth and stable rotational trajectory, the SMC-NSM method generates larger oscillations before convergence. This phenomenon originates from the discontinuous switching characteristic of sliding-mode control, which often introduces chattering effects in practical systems. Since cable-driven parallel robots are highly sensitive to attitude variations, such oscillations may lead to undesirable cable tension fluctuations and reduced positioning accuracy.

The numerical results in Table 1 strongly support this analysis. Under ideal conditions, the proposed controller reduces the RMSE of ϕ_z to $3.6575 \cdot 10^{-4}$ rad, whereas the SMC-NSM method yields $5.0935 \cdot 10^{-4}$ rad. Similarly, the proposed strategy significantly decreases the RMSE values of ϕ_x and ϕ_y , demonstrating enhanced rotational stabilization capability. Moreover, the maximum angular errors are also substantially reduced, confirming that the proposed controller effectively attenuates transient rotational fluctuations. This setup ensures a consistent and unbiased evaluation of the control performance for the 8-CDPR system.

The three-dimensional trajectory tracking results shown in Figure 4 further validate the effectiveness of the proposed approach. The actual trajectory generated by the proposed controller almost perfectly overlaps the desired reference trajectory throughout the entire motion path. Although the SMC-NSM controller is also capable of tracking the reference, small deviations remain observable in curved trajectory segments where the system dynamics become highly coupled. The proposed method therefore demonstrates superior spatial tracking consistency and better synchronization between translational and rotational motions.

Under noisy operating conditions, the superiority of the

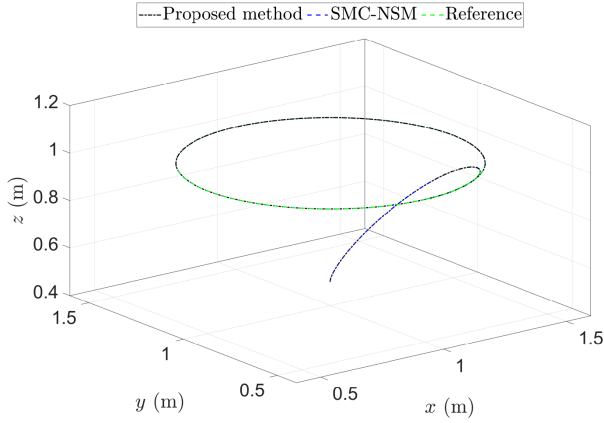


Figure 4: Case 1: Trajectory tracking performance of the system under the proposed method and SMC-NSM compared with the reference trajectory.

Control Method	Variable	ME	RMSE
Proposed Method	x (m)	$8.739 \cdot 10^{-4}$	$2.8566 \cdot 10^{-4}$
	y (m)	$6.1049 \cdot 10^{-4}$	$2.2338 \cdot 10^{-4}$
	z (m)	$6.5141 \cdot 10^{-4}$	$1.7951 \cdot 10^{-4}$
	ϕ_x (rad)	$2.6193 \cdot 10^{-8}$	$4.9913 \cdot 10^{-9}$
	ϕ_y (rad)	$1.8081 \cdot 10^{-6}$	$3.7123 \cdot 10^{-7}$
	ϕ_z (rad)	0.0016	$3.6575 \cdot 10^{-4}$
	SMC-based Null Space Method	x (m)	0.0011
y (m)		$8.2262 \cdot 10^{-4}$	$3.2661 \cdot 10^{-4}$
z (m)		$8.966 \cdot 10^{-4}$	$2.4527 \cdot 10^{-4}$
ϕ_x (rad)		$5.033 \cdot 10^{-5}$	$2.8718 \cdot 10^{-5}$
ϕ_y (rad)		$5.033 \cdot 10^{-5}$	$2.7998 \cdot 10^{-5}$
ϕ_z (rad)		0.0022	$5.0935 \cdot 10^{-4}$

Table 1: Case 1: Performance comparison of controllers using error indices.

proposed controller becomes significantly more evident, particularly in terms of robustness, disturbance attenuation capability, and chattering suppression. As illustrated in Figures 5 and 6, the presence of disturbances and measurement noise affects both controllers; however, the degradation in performance observed in the proposed method remains substantially smaller than that of the SMC-NSM controller.

From the tracking responses in Figure 5, it can be observed that the proposed controller maintains highly accurate trajectory tracking despite the injected disturbances and sensor noise. Although small fluctuations appear around the reference trajectories, the actual responses remain smooth and tightly bounded throughout the entire simulation interval. In contrast, the SMC-NSM controller exhibits visibly larger oscillations, especially during regions where the trajectory curvature changes rapidly or when the velocity direction reverses. This behavior indicates that the conventional sliding-mode-based approach is more sensitive to measurement perturbations and external disturbances.

A more detailed observation of the zoomed-in regions provides additional insight into the robustness characteristics of the proposed strategy. In the x -axis response, the proposed controller maintains extremely small local deviations even during transient phases. The error evolution remains smooth without

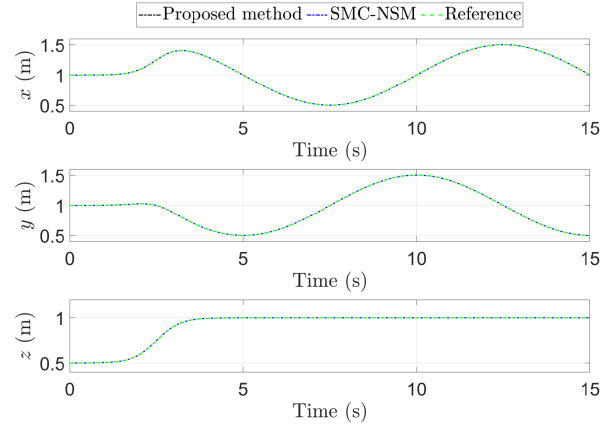


Figure 5: Case 2: Translational motions of the cable-driven parallel robot in the scenario affected by external disturbances.

exhibiting abrupt oscillatory behavior. Meanwhile, the SMC-NSM controller produces noticeable fluctuations around the reference trajectory, indicating that disturbance propagation is insufficiently attenuated inside the closed-loop system.

This phenomenon is confirmed by the RMSE results presented in Table 2. Under noisy conditions, the proposed controller achieves an RMSE of $2.8396 \cdot 10^{-4}$ m in the x -direction, while the SMC-NSM method increases to $4.8851 \cdot 10^{-4}$ m.

A similar trend can be observed in the y -direction. The proposed controller preserves smooth convergence and avoids high-frequency oscillations despite continuous disturbance injection. The SMC-NSM controller, however, exhibits residual fluctuations near the steady-state region, indicating incomplete suppression of noise-induced perturbations. The RMSE is reduced from $4.2774 \cdot 10^{-4}$ m using the SMC-NSM method to $2.7431 \cdot 10^{-4}$ m using the proposed controller. This improvement confirms that the proposed strategy enhances not only transient performance but also long-term steady-state accuracy under uncertain operating conditions.

The robustness advantage becomes even more meaningful in the z -direction. In cable-driven parallel robots, vertical motion is strongly affected by gravitational loading, cable tension redistribution, and nonlinear coupling effects. Consequently, disturbances in this direction generally produce stronger dynamic impacts. Despite these challenges, the proposed controller maintains stable vertical tracking with very small oscillatory amplitudes. The RMSE remains at $2.2947 \cdot 10^{-4}$ m, which is still lower than the $3.3551 \cdot 10^{-4}$ m achieved by the SMC-NSM method. More importantly, the proposed controller exhibits smoother error evolution and reduced transient peaks, indicating better dynamic compensation capability under external perturbations.

In practical cable-driven robotic systems, rotational dynamics are considerably more sensitive to disturbances because even small angular deviations can lead to substantial variations in cable tensions and platform stability. Therefore, maintaining smooth attitude regulation under noisy conditions is critically important.

For the ϕ_x response, the proposed controller maintains an almost noise-free tracking behavior with only very small fluctuations around the equilibrium point. In contrast, the SMC-NSM controller exhibits persistent oscillatory behavior throughout the simulation interval. These oscillations originate

from the discontinuous switching nature of sliding-mode control, which amplifies high-frequency noise components and generates chattering phenomena.

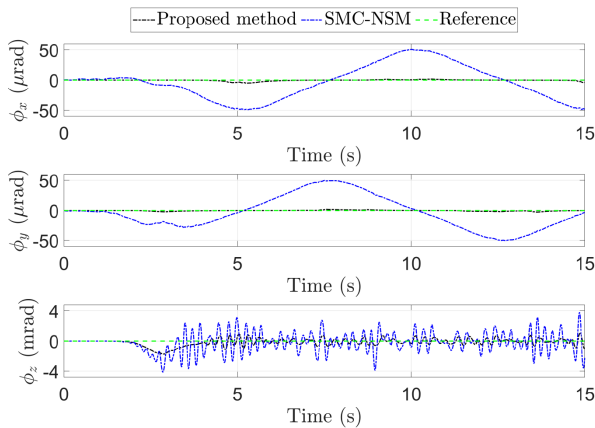


Figure 6: Case 2: Rotational motions of the cable-driven parallel robot in the scenario affected by external disturbances.

This difference is quantitatively reflected in the RMSE values. The proposed controller reduces the RMSE of ϕ_x to $1.2628 \cdot 10^{-6}$ rad, whereas the SMC-NSM controller produces $2.9491 \cdot 10^{-5}$ rad. This corresponds to an error reduction of more than one order of magnitude, demonstrating the superior capability of the proposed strategy in suppressing rotational disturbances.

A similar behavior can be observed in the ϕ_y response. The proposed method maintains stable angular tracking with minimal oscillatory behavior even under continuous disturbance injection. Conversely, the SMC-NSM controller suffers from visible oscillations that persist throughout the simulation process. The RMSE is reduced from $2.8653 \cdot 10^{-5}$ rad to $8.1807 \cdot 10^{-7}$ rad, which again confirms the strong robustness and noise attenuation capability of the proposed framework.

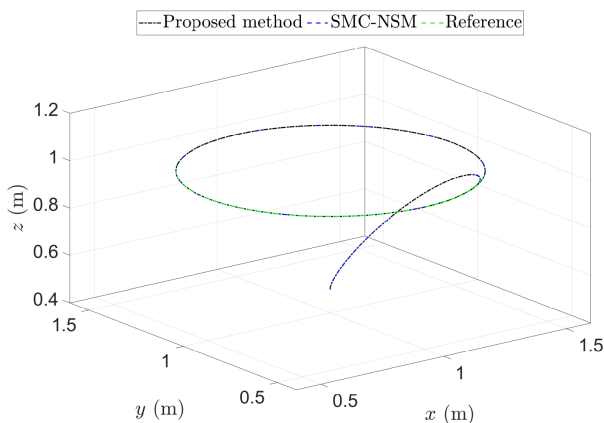


Figure 7: Case 2: Trajectory tracking performance of the system under the proposed method and SMC-NSM compared with the reference trajectory in the presence of external disturbances.

The three-dimensional trajectory tracking performance under noisy conditions, illustrated in Figure 7, further demonstrates the robustness and stability of both control strategies. Despite the presence of external disturbances and measurement noise, both the proposed controller and the SMC-NSM method are still capable of following the desired spatial tra-

jectory with relatively high accuracy. The actual trajectories generated by both controllers remain very close to the reference path throughout the motion process, indicating that the overall closed-loop system stability is preserved even under uncertain operating conditions.

Control Method	Variable	ME	RMSE
Proposed Method	x (m)	$9.4353 \cdot 10^{-4}$	$2.8396 \cdot 10^{-4}$
	y (m)	$7.9204 \cdot 10^{-4}$	$2.7431 \cdot 10^{-4}$
	z (m)	$8.8537 \cdot 10^{-4}$	$2.2947 \cdot 10^{-4}$
	ϕ_x (rad)	$5.0883 \cdot 10^{-6}$	$1.2628 \cdot 10^{-6}$
	ϕ_y (rad)	$2.5236 \cdot 10^{-6}$	$8.1807 \cdot 10^{-7}$
SMC-based Null Space Method	ϕ_z (rad)	0.0018	$4.9686 \cdot 10^{-4}$
	x (m)	0.0038	$4.8851 \cdot 10^{-4}$
	y (m)	$8.749 \cdot 10^{-4}$	$4.2774 \cdot 10^{-4}$
	z (m)	$9.2275 \cdot 10^{-4}$	$3.3551 \cdot 10^{-4}$
	ϕ_x (rad)	$5.0192 \cdot 10^{-5}$	$2.9491 \cdot 10^{-5}$
	ϕ_y (rad)	$5.0175 \cdot 10^{-5}$	$2.8653 \cdot 10^{-5}$
	ϕ_z (rad)	0.0041	0.0013

Table 2: Case 2: Performance comparison of controllers using error indices.

Although the quantitative error indices presented in Table 2 confirm that the proposed controller achieves lower ME and RMSE values than the SMC-NSM approach, the results in Figure 7 show that both controllers are still able to accomplish the prescribed three-dimensional trajectory successfully. In other words, the injected disturbances and measurement noise do not significantly deteriorate the overall spatial tracking capability of the system. Nevertheless, the proposed method maintains a smoother and more consistent trajectory with smaller local deviations, reflecting its superior disturbance rejection and robustness performance.

5. Conclusion

This study has developed a complete dynamic model of a 6-DOF eight-cable-driven parallel robot to describe both translational and rotational motions of the end-effector. Based on this model, a hybrid control strategy combining Sliding Mode Control (SMC) and Bounded Variable Least Squares (BVLS) has been developed to simultaneously achieve robust trajectory tracking and feasible cable tension distribution. The simulation results under nominal operating conditions show that the proposed method achieves fast response characteristics with accurate trajectory tracking performance for the desired positions and orientation angles. In addition, the system exhibits negligible steady-state error while maintaining small angular deviations throughout the motion process. Furthermore, all cable tensions remain within the bounded constraints imposed by the BVLS algorithm. Additional simulations under external disturbances also demonstrate that the proposed controller maintains satisfactory tracking performance and robustness against disturbances. Therefore, the proposed approach demonstrates its effectiveness for stable and constrained control of cable-driven parallel robots.

Although the proposed SMC-BVLS framework has demonstrated effective trajectory tracking and feasible cable tension allocation, this study still has several limitations. First, the validation was mainly conducted through numerical simu-

lations, while experimental verification on a real eight-cable-driven parallel robot has not yet been performed. In addition, some practical factors, such as cable elasticity, cable sagging, pulley friction, actuator dynamics, sensor noise characteristics, and payload variations, were simplified or neglected in the current model. These factors may influence tracking accuracy and tension distribution in real-time applications. Therefore, future research will focus on implementing the proposed controller on an experimental CDPR platform, considering more realistic cable and actuator dynamics, and evaluating the control performance under different payloads, trajectories, and disturbance conditions. Moreover, adaptive or optimal tuning strategies can be integrated with the SMC-BVLS framework to further improve robustness, reduce chattering, and enhance real-time control efficiency.

References

- [1] B. Zhang, W. Shang, S. Cong, and Z. Li, "Dual-loop dynamic control of cable-driven parallel robots without online tension distribution," *IEEE Transactions on Systems, Man, and Cybernetics: Systems*, vol. 52, no. 10, pp. 6555–6568, 2022.
- [2] E. Idà, S. Briot, and M. Carricato, "Natural oscillations of underactuated cable-driven parallel robots," *IEEE Access*, vol. 9, pp. 71 660–71 672, 2021.
- [3] J. Kang, K. Ghonasgi, C. J. Walsh, and S. K. Agrawal, "Simulating hemiparetic gait in healthy subjects using tpad with a closed-loop controller," *IEEE Transactions on Neural Systems and Rehabilitation Engineering*, vol. 27, no. 5, pp. 974–983, 2019.
- [4] Z. Zhao, L. Zhang, H. Nan, and B. Wang, "System modeling and motion control of a cable-driven parallel platform for underwater camera stabilization," *IEEE Access*, vol. 9, pp. 132 954–132 966, 2021.
- [5] B. Zhang, W. Shang, and S. Cong, "Synchronous impedance control of cable-driven parallel robots with external interaction," *IEEE/ASME Transactions on Mechatronics*, 2025.
- [6] M. Zarebidoki, J. S. Dhupia, and W. Xu, "A review of cable-driven parallel robots: Typical configurations, analysis techniques, and control methods," *IEEE Robotics & Automation Magazine*, vol. 29, no. 3, pp. 89–106, 2022.
- [7] Q. Chen, B. Zi, Z. Sun, Y. Li, and Q. Xu, "Design and development of a new cable-driven parallel robot for waist rehabilitation," *IEEE/ASME Transactions on Mechatronics*, vol. 24, no. 4, pp. 1497–1507, 2019.
- [8] D.-C. Nguyen, D.-H. Nguyen, Q.-T. Dao, and T.-V.-A. Nguyen, "Trajectory tracking and orientation stability of planar cable robots using pso-tuned sliding mode control," in *International Conference on Interactive Collaborative Robotics*, Springer, 2025, pp. 321–333.
- [9] F. Xie, W. Shang, B. Zhang, S. Cong, and Z. Li, "High-precision trajectory tracking control of cable-driven parallel robots using robust synchronization," *IEEE Transactions on Industrial Informatics*, vol. 17, no. 4, pp. 2488–2499, 2020.
- [10] M. A. Khosravi and H. D. Taghirad, "Robust pid control of fully-constrained cable driven parallel robots," *Mechatronics*, vol. 24, no. 2, pp. 87–97, 2014.
- [11] S. Nguyen-Van, D. T. T. Thuy, N. N. T. Thanh, and N. N. Dinh, "Evolutionary tuning of pid controllers for a spatial cable-driven parallel robot," in *International Conference on Engineering Research and Applications*, Springer, 2020, pp. 411–424.
- [12] H. Jamshidifar, B. Fidan, G. Gungor, and A. Khajepour, "Adaptive vibration control of a flexible cable driven parallel robot," *IFAC-PapersOnLine*, vol. 48, no. 3, pp. 1302–1307, 2015.
- [13] B. Zi, B. Duan, J. Du, and H. Bao, "Dynamic modeling and active control of a cable-suspended parallel robot," *Mechatronics*, vol. 18, no. 1, pp. 1–12, 2008.
- [14] M. Carpio, R. Saltaren, J. Viola, C. Calderon, and J. Guerra, "Proposal of a decoupled structure of fuzzy-pid controllers applied to the position control in a planar cdpr," *Electronics*, vol. 10, no. 6, p. 745, 2021.
- [15] H. Xiong, L. Zhang, and X. Diao, "A learning-based control framework for cable-driven parallel robots with unknown jacobians," *Proceedings of the Institution of Mechanical Engineers, Part I: Journal of Systems and Control Engineering*, vol. 234, no. 9, pp. 1024–1036, 2020.
- [16] H. Chen, M.-C. Kim, Y. Ko, and C.-S. Kim, "Compensated motion and position estimation of a cable-driven parallel robot based on deep reinforcement learning," *International Journal of Control, Automation and Systems*, vol. 21, no. 11, pp. 3507–3518, 2023.
- [17] E. Oghabi, R. K. Moghaddam, and H. R. Kobravi, "Adaptive interval type-2 fuzzy neural network nonsingular fast terminal sliding mode control for cable-driven parallel robots," *Engineering Applications of Artificial Intelligence*, vol. 136, p. 108 963, 2024.
- [18] C. Sancak, M. Itik, and T. T. Nguyen, "Position control of a fully constrained planar cable-driven parallel robot with unknown or partially known dynamics," *IEEE/ASME Transactions on Mechatronics*, vol. 28, no. 3, pp. 1605–1615, 2023.
- [19] Y. Lu, C. Wu, W. Yao, G. Sun, J. Liu, and L. Wu, "Deep reinforcement learning control of fully-constrained cable-driven parallel robots," *IEEE Transactions on Industrial Electronics*, vol. 70, no. 7, pp. 7194–7204, 2022.
- [20] B. Zhou, Y. Wang, B. Zi, and W. Zhu, "Fuzzy adaptive whale optimization control algorithm for trajectory tracking of a cable-driven parallel robot," *IEEE Transactions on Automation Science and Engineering*, vol. 21, no. 4, pp. 5149–5160, 2023.
- [21] T.-V.-A. Nguyen, T.-L. Nguyen, and M.-L. Nguyen, "Optimization of sliding mode controller parameters for planar parallel robot," *Journal of Measurement, Control and Automation*, vol. 29, no. 1, pp. 58–65, 2025.
- [22] N. T. Le and T. L. Nguyen, "Designing sliding mode control using exponential functions applied for the 5-dof vnr t1 robot," *Journal of Measurement, Control and Automation*, vol. 1, no. 1, 2020.
- [23] M. Zhang, Y. Zhang, H. Chen, and X. Cheng, "Model-independent pd-smc method with payload swing suppression for 3d overhead crane systems," *Mechanical Systems and Signal Processing*, vol. 129, pp. 381–393, 2019.
- [24] S. Mahjoub, S. Labdai, L. Chrifi-Alaoui, S. Drid, and N. Derbel, "Design and implementation of a fuzzy logic supervisory based on smc controller for a dual input-single output converter," *International Journal of Electrical Power & Energy Systems*, vol. 150, p. 109 053, 2023.
- [25] X. Shi et al., "Adaptive fractional-order smc controller design for unmanned quadrotor helicopter under actuator fault and disturbances," *Ieee Access*, vol. 8, pp. 103 792–103 802, 2020.
- [26] M. R. Mousavi, M. Ghanbari, S. A. A. Moosavian, and P. Zarafshan, "Rapid and safe wire tension distribution scheme for redundant cable-driven parallel manipulators," *Robotica*, vol. 40, no. 7, pp. 2395–2408, 2022.
- [27] M. Fabritius, G. Rubio-Gomez, C. Martin, J. C. Santos, W. Kraus, and A. Pott, "A nullspace-based force correction method to improve the dynamic performance of cable-driven parallel robots," *Mechanism and Machine Theory*, vol. 181, p. 105 177, 2023.
- [28] A. Rodriguez-Barroso, R. Saltaren, G. A. Portilla, J. S. Cely, and M. Carpio, "Cable-driven parallel robot with reconfigurable end effector controlled with a compliant actuator," *Sensors*, vol. 18, no. 9, p. 2765, 2018.
- [29] D.-C. Nguyen et al., "Fixed-time active fault-tolerant control for cable-driven robots under tension constraints," *European Journal of Control*, p. 101 503, 2026.
- [30] N. Saraf and A. Bemporad, "A bounded-variable least-squares solver based on stable qr updates," *IEEE transactions on automatic control*, vol. 65, no. 3, pp. 1242–1247, 2019.
- [31] S.-H. Hou, X.-Q. Tang, L. Cao, Z.-W. Cui, H.-N. Sun, and Y.-W. Yan, "Research on end-force output of 8-cable driven parallel manipulator," *International Journal of Automation and Computing*, vol. 17, no. 3, pp. 378–389, 2020.
- [32] R. J. Hanson, "Linear least squares with bounds and linear constraints," *SIAM Journal on scientific and statistical computing*, vol. 7, no. 3, pp. 826–834, 1986.